Advances in Geo-Energy Research

Vol. 17, No. 2, p. 95-106, 2025

Original article

Investigating rock properties and fracture propagation pattern during supercritical CO_2 pre-fracturing in conglomerate reservoir

Hang Zhou[1,3], Tingwei Yan[2], Japan Trivedi[3], Bo Wang[2]*, Fujian Zhou[1]

[1]*State Key Laboratory of Petroleum Resources and Engineering, China University of Petroleum, Beijing 102249, P. R.China*

[2]*College of Petroleum, China University of Petroleum-Beijing at Karamay, Karamay 834000, P. R. China*

[3]*Faculty of Engineering-Civil and Environmental Engineering, University of Alberta, Edmonton, Alberta T6G 2R3, Canada*

Keywords:
Physicochemical mechanisms
conglomerate
CO_2 soaking
true triaxial fracturing
field-scale application

Cited as:
Zhou, H., Yan, T., Trivedi, J., Wang, B., Zhou, F. Investigating rock properties and fracture propagation pattern during supercritical CO_2 pre-fracturing in conglomerate reservoir. Advances in Geo-Energy Research, 2025, 17(2): 95-106.
https://doi.org/10.46690/ager.2025.08.02

Abstract:
Carbon dioxide pre-fracturing has shown high application potential in improving oil recovery in conglomerate reservoirs. However, the influence of CO_2 on the physical properties of reservoir rock and its diffusion behavior within the reservoir matrix have not been systematically studied. This paper integrates CO_2-saturated water soaking experiments, true triaxial fracturing experiments and field-scale tests to demonstrate that CO_2 soaking induces quartz reduction and clay mineral increase, leading to a decrease in porosity and mechanical strength. Clay-cemented conglomerates experience a greater loss in compressive strength and a higher reduction in permeability compared to calcareous-cemented counterparts under identical CO_2 soaking. In the horizontal principal stress direction, CO_2 fracturing achieves a greater fracture penetration depth than slickwater fracturing or CO_2 pre-injection followed by slickwater fracturing. CO_2 pre-fracturing reduces breakdown pressure by 15%-5% and increases fracture complexity. Field tests confirm a reduction in injection pressure and improved effective stimulation. However, dnarrower fracture width and higher tortuosity may limit proppant transportation.

1. Introduction

The pronounced mechanical heterogeneity and complex pore structure of tight conglomerate reservoirs pose substantial challenges in reservoir development, since gravel particle size (Boggs, 2014; Khanlari et al., 2016; Zhou et al., 2025), content and distribution, along with mechanical disparities between gravels and the matrix, significantly influence artificial fracture propagation (Fairhurst, 1964; Haimson, 2007; Kar and Chaudhuri, 2024). Gravels contain quartz, K-feldspar, plagioclase (Warren et al., 1983), and water-sensitive clay minerals that undergo swelling (Barnaji et al., 2016) and migrate (De Silva et al., 2017) when exposed to conventional water-based fracturing fluids. These processes cause pore blockage, permeability reduction (Liu et al., 2020) and severe formation damage due to high water consumption (Galdeano et al., 2017; Wu et al., 2021), necessitating optimized fracturing fluid selection for efficient reservoir stimulation (Trivedi and Babadagli, 2008; Agrawal and Sharma, 2015).

Continuous CO_2 injection initiates interactions with reservoir rocks, causing mineral dissolution and secondary precipitation, which in turn modify pore structures and influence reservoir fluid migration (Al-Yaseri et al., 2022; Abes and Michael, 2025). Under geological CO_2 storage conditions, simulations have demonstrated that CO_2 reacts with water to form carbonic acid, which lowers fluid pH and indirectly promotes the dissolution of aluminosilicate minerals such as

Yandy Scientific Press

*Corresponding author.
E-mail address: 2023311224@student.cup.edu.cn (H. Zhou); weitingyan2000@163.com (T. Yan); jtrivedi@ualberta.ca (J. Trivedi); wangbo@cupk.edu.cn (B. Wang); zhoufj@cup.edu.cn (F. Zhou).
2207-9963 © The Author(s) 2025.
Received June 3, 2025; revised June 27, 2025; accepted July 13, 2025; available online July 16, 2025.

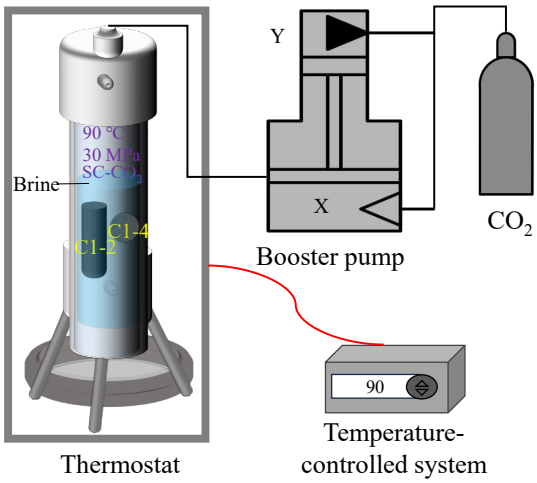

Fig. 1. Experimental equipment.

plagioclase (Min and Jun, 2016). Microscopic laboratory observations further confirm the structural alterations, notably significant feldspar dissolution and the localized expansions of pores and microfractures (Patton et al., 2003; Mukhametdinova et al., 2024). To study these phenomena, researchers have developed a reactive transport model that combines chemical thermodynamics and kinetics. The results showed that CO_2-water-conglomerate interactions increase pore-throat sizes through mineral dissolution and migration, enhancing connectivity and seepage capacity, while secondary mineral precipitation may locally obstruct pores (Kanakiya et al., 2017).

Recent studies have clarified the impact of continuous CO_2 injection on reservoir fracture evolution. True triaxial fracturing experiments were conducted to demonstrate that CO_2-induced breakdown pressures are significantly lower than predictions based on a pore elasticity model and measurements using water-based fracturing fluids (Ha et al., 2018; Feng and Firoozabadi, 2023; Chen et al., 2024). Additionally, higher supercritical CO_2 pressures within fractures significantly enhance branch fracture formation (Li et al., 2021). Field tests performed on shale oil reservoirs in the Jiyang Depression of the Bohai Bay Basin further validated these simulations by indicating that CO_2 injection reduces breakdown pressures, promotes effective fluid loss along bedding planes, induces complex fracture networks, and increases formation energy (Li et al., 2024).

Conglomerate reservoirs face three principal engineering and geological challenges during CO_2 fracturing:

1) Multi-mineral components exhibit distinct dissolution kinetics (Al Kalbani et al., 2024);
2) Multi-scale heterogeneity exists at the gravel-matrix interface (Huang et al., 2023);
3) The type and strength of cementation critically influence the reservoir's mechanical response (Wang et al., 2022).

Thus far, the physicochemical coupling mechanisms in conglomerate reservoirs under CO_2 exposure have not been systematically quantified. To elucidate the multifaceted impacts of CO_2 on mineralogy, pore architecture, mechanical attributes, and fracture propagation across distinct conglomerate types, this study uniquely integrates CO_2-saturated water soaking experiments and precision triaxial fracturing tests, and the underlying coupling mechanisms of CO_2 fracturing are systematically decoded. The core innovations of this work are as follows:

1) The synergistic CO_2-induced damage effects-mineral dissolution and mechanical weakening-in conglomerates with varying support and cementation types are quantitatively delineated for the first time;
2) Quantitative correlations between fracture propagation patterns and support/cementation characteristics during CO_2 pre-fracturing are established for different conglomerate classes;
3) The physicochemical coupling mechanism of CO_2 fracturing is comprehensively unveiled through a synergistic integration of laboratory-derived insights and field-scale data.

2. Materials and methods

2.1 Samples

The core samples were collected from the Upper Wuerhe Formation and Baikouquan Formation of the conglomerate reservoir in the northwestern Junggar Basin, Xinjiang. The experiments included CO_2-saturated brine soaking of conglomerate and true triaxial fracturing tests. To accurately simulate the chemical dissolution effect of CO_2 on the conglomerate and its fracturing performance, three types of samples were drilled from the same full-diameter core: (a) 8 cm × 8 cm × 10 cm samples for true triaxial fracturing experiments; (b) 2.5 cm × 5 cm samples for CO_2-saturated soaking experiments to measure porosity, permeability, compressive strength, Young's modulus, Poisson's ratio, and mineral composition before and after soaking; and (c) 2.5 cm × 1.5 cm samples for CO_2-saturated soaking experiments to measure tensile strength before and after soaking.

According to the analysis report of water quality of the conglomerate reservoir, the synthetic brine was prepared for the static soaking experiments with distilled water, and its composition (wt.%) was 0.5% KCl, 1.99% NaCl, 0.02% $MgCl_2$, and 0.15% $CaCl_2$.

2.2 Methods

The soaking equipment is shown in Fig. 1. Cylindrical samples (2.5 cm × 5 cm; C1-2, C4-2, C5-2, C6-2) were measured for porosity, permeability, and Nuclear Magnetic Resonance (NMR) response. The core surface morphology was also observed using high-magnification scanning electron microscopy. Samples were placed into the high-temperature, high-pressure vessel. The prepared brine was introduced into the boat and CO_2 was injected through a pipeline, setting the injection pressure to 30 MPa. The vessel was placed in a thermostatic oven at 90 °C and soaked for 24 h. After soaking, the samples were dried, followed by conducting tests for porosity, permeability, NMR, triaxial compression, and Brazilian splitting. The core surface morphology was observed via high-magnification scanning electron microscopy, and po-

Table 1. Schemes of the static soaking experiments.

No.	Temperature (°C)	Pressure (MPa)
C1-2	90	30
C1-3	/	/
C1-4	90	30
C1-5	/	/
C4-2	90	30
C4-3	/	/
C4-4	90	30
C4-5	/	/
C5-2	90	30
C5-3	/	/
C5-4	90	30
C5-5	/	/
C6-2	90	30
C6-3	/	/
C6-4	90	30
C6-5	/	/

Table 2. Schemes of the fracturing experiments.

No.	Static soaking (24 h)	Fracturing media
C1-1	CO_2-saturated brine	SC-CO_2
C2-1	/	SC-CO_2 + Slickwater
C3-1	/	Slickwater
C4-1	CO_2-saturated brine	SC-CO_2
C5-1	CO_2-saturated brine	SC-CO_2
C6-1	CO_2-saturated brine	SC-CO_2

wder samples were prepared for X-Ray Diffraction analysis. On the basis of the test results, the effects of CO_2-saturated water on the mineral composition of different conglomerate support types was analyzed, along with its influence on pore structure characteristics. The details of the soaking experimental scheme are presented in Table 1.

Table 2 summarizes the experimental fracturing schemes: C1-1 with direct CO_2 fracturing and C2-1 with CO_2 pre-injection followed by slickwater fracturing. Before fracturing, the C1-1, C4-1, C5-1, and C6-1 samples were soaked in CO_2-saturated brine for 24 h to simulate the chemical dissolution effects of CO_2-saturated water. The samples were dried and the cores were embedded with epoxy resin after soaking. The conglomerate samples were loaded into the triaxial loading frame, followed by applying triaxial stress ($\sigma_v/\sigma_H/\sigma_h = 18/28/25$ MPa). CO_2 or fracturing fluid was injected at 10 mL/min until a distinct pressure drop occurred, when the injection was terminated. The internal fracture morphology was characterized by CT scanning and 3D reconstruction, and microscopic fracture development was observed using scanning electron microscopy.

Table 3. Changes in rock and clay mineral compositions.

Type	Mineral	C1	C4	C5	C6
Rock	Quartz	+1.5	+1.6	+2.1	+2.9
	K-feldspar	-1.7	-0.5	-0.6	-2.5
	Plagioclase	+3.2	-4.0	-3.9	+0.3
	Clay	-3.0	+2.9	+2.4	+1.8
Clay	I/S	+6.0	+8.0	+13.0	/
	Illite	-6.0	-4.0	-4.0	-10.0
	Kaolinite	+3.0	+5.0	+5.0	+15.0
	Chlorite	-3.0	-9.0	-14.0	-5.0

Notes: "+" indicates an increase, and "-" indicates a decrease.

3. Results

3.1 Chemical dissolution

3.1.1 Changes in mineral composition

After soaking, the contents of K-feldspar and plagioclase decreased significantly, while the clay mineral and quartz content increased markedly. The illite content increased, the kaolinite content decreased, the chlorite content increased, and the Illite/Smectite (I/S) mixed-layer content decreased significantly in C1 and C4 (Table 3). In the C5 core, both the illite and kaolinite contents decreased slightly, while the chlorite content increased significantly. In the C6 core, the illite and kaolinite contents decreased slightly, the chlorite content remained unchanged, and the I/S mixed-layer content increased (Perera et al., 2011; de Jong et al., 2014). Differences in the magnitude of mineral composition changes were also observed between particle-supported conglomerates and multi-size particle-supported conglomerates. The decrease in quartz content and the increase in clay content were more pronounced in particle-supported conglomerates. It has been established that the clay mineral content increases more in clay-cemented conglomerates than in calcite-cemented conglomerates (Rathnaweera et al., 2017).

3.1.2 Changes in porosity and permeability

After soaking, the porosity of all conglomerate types demonstrated a significant decrease (Table 4). The most pronounced porosity reduction occurred in calcite-cemented conglomerate (C6-2), likely attributable to substantial secondary mineral precipitation following carbonate mineral dissolution. Both porosity and permeability decreased markedly in clay-cemented conglomerates (C1-2, C4-2, C5-2). C1-2 had the lowest absolute porosity but exhibited the most significant permeability reduction, indicating that clay mineral swelling and secondary mineral precipitation induce severe pore throat

Table 4. Changes in porosity and permeability.

Rock properties	C1	C4	C5	C6
Porosity (%)	-0.717	-1.156	-0.694	-1.979
Permeability (mD)	-0.387	-1.216	-0.687	-0.006

Notes: "+" indicates an increase, and "-" indicates a decrease.

Table 5. Changes in mechanical properties.

Rock properties	C1	C4	C5	C6
Compressive strength (MPa)	-1.43	-36.58	-26.44	-24.49
Tensile strength (MPa)	-0.88	-0.55	-0.89	-0.68
Young's modulus (GPa)	-7.44	-1.91	-1.49	-2.36
Poisson's ratio (-)	+0.03	+0.01	+0.03	+0.01

Notes: "+" indicates an increase, and "-" indicates a decrease.

blockage in clay-cemented conglomerates, leading to a pronounced permeability decline. In calcite-cemented conglomerate (C6-2), the porosity reduction was the largest, but the initial permeability was extremely low. This suggests that although calcite-cemented conglomerate is prone to dissolution, secondary mineral precipitation impairs pore connectivity to a greater extent. Overall, CO_2-saturated water soaking significantly degrades the pore structure of conglomerate reservoirs, reducing both porosity and permeability (Nooraiepour et al., 2025).

3.1.3 Changes in mechanical properties

All conglomerate types exhibited a decrease in compressive strength after soaking, with significant variation in the reduction degree (Table 5). This reduction in compressive strength is primarily attributed to mineral composition changes and pore structure damage, particularly in clay-cemented conglomerates, where significant mineral dissolution and secondary mineral formation weaken the internal framework. In calcite-cemented conglomerates, although substantial carbonate mineral dissolution occurred during soaking and structural weakening was evident, the relative reduction remained moderate.

All conglomerate types also exhibited a significant decrease in tensile strength after soaking. Clay-cemented conglomerates (C1-2, C4-2, C5-2) showed more pronounced reductions in both compressive and tensile strength, with the mixed matrix-particle-supported clay-cemented conglomerate (C4-2) exhibiting the most significant compressive strength decrease. Calcite-cemented conglomerate (C6-2) had the highest initial compressive strength; although its reduction was notable, the absolute strength remained relatively high, reflecting better structural stability and mechanical resistance. These results suggest that CO_2-saturated water induces varying degrees of mechanical damage in conglomerates with different cementation types, and clay-cemented conglomerates are more sensitive to CO_2 soaking. In contrast, calcite-cemented conglomerates maintain higher mechanical stability despite some dissolution.

All conglomerate types exhibited a decrease in Young's modulus, indicating reduced elastic deformation capacity and rigidity. This reduction is likely attributed to mineral dissolution, local cementation damage within the conglomerate, and alterations in the mineral composition and secondary mineral formation, which weaken the overall elasticity and structural integrity of the rock.

A general increase in Poisson's ratio was observed, indicating enhanced lateral deformation and reduced structural toughness. An increase in Poisson's ratio is typically associated with local pore structure collapse or closure following mineral dissolution, as well as an increased content and swelling of soft minerals (particularly clay minerals), which enhance the tendency for lateral deformation.

C1-2 exhibited the most significant decrease in Young's modulus and a notable increase in Poisson's ratio, indicating that particle-supported conglomerate experiences the most substantial reduction in elastic stiffness and the most significant increase in lateral deformation. C5-2 showed a minor decrease in Young's modulus albeit the most pronounced increase in Poisson's ratio, indicating that changes in internal porosity significantly influence lateral deformation in matrix-particle-supported conglomerates. C6-2 displayed relatively small changes in both Young's modulus and Poisson's ratio, reflecting better structural stability and deformation resistance, which may be attributed to the relative stability of calcite minerals. These results demonstrate that CO_2-saturated water significantly affects the elastic properties of conglomerates; especially, it reduces the elastic deformation capacity of clay-cemented conglomerates.

3.2 Physicochemical coupling

C1-1 exhibited numerous tortuous fractures bypassing gravels in gravel-rich zones with narrow widths. Within larger gravels, some crossing fractures exhibited significant tortuosity and deflection within the gravel. Highly dispersed fractures were observed in C1-1 with considerable tortuosity. Due to the presence of gravel, most fractures propagate by bypassing gravels, leading to poor continuity of the fracture network. During CO_2 fracturing, significant pressure fluctuations could be observed on the pressure response curve, indicating multiple fracture initiation events. This further confirms the presence of numerous branch fractures, as observed in the fracture morphology.

C2-1 exhibited a complex fracture network with dense fractures near the wellbore. The main fracture was wide, and fractures in gravel-rich zones predominantly propagated around gravels. A main fracture and multiple branch fractures formed along the maximum horizontal principal stress direction. The main fracture exhibited low tortuosity and good continuity. The breakdown pressure of CO_2 fracturing was notably lower than that of slickwater fracturing. The lower viscosity of CO_2 enables easier penetration into the core than water-based fracturing fluids, allowing mechanical damage and fracture initiation to occur preferentially at weaker stress points within the core (Ishida et al., 2016). Pronounced

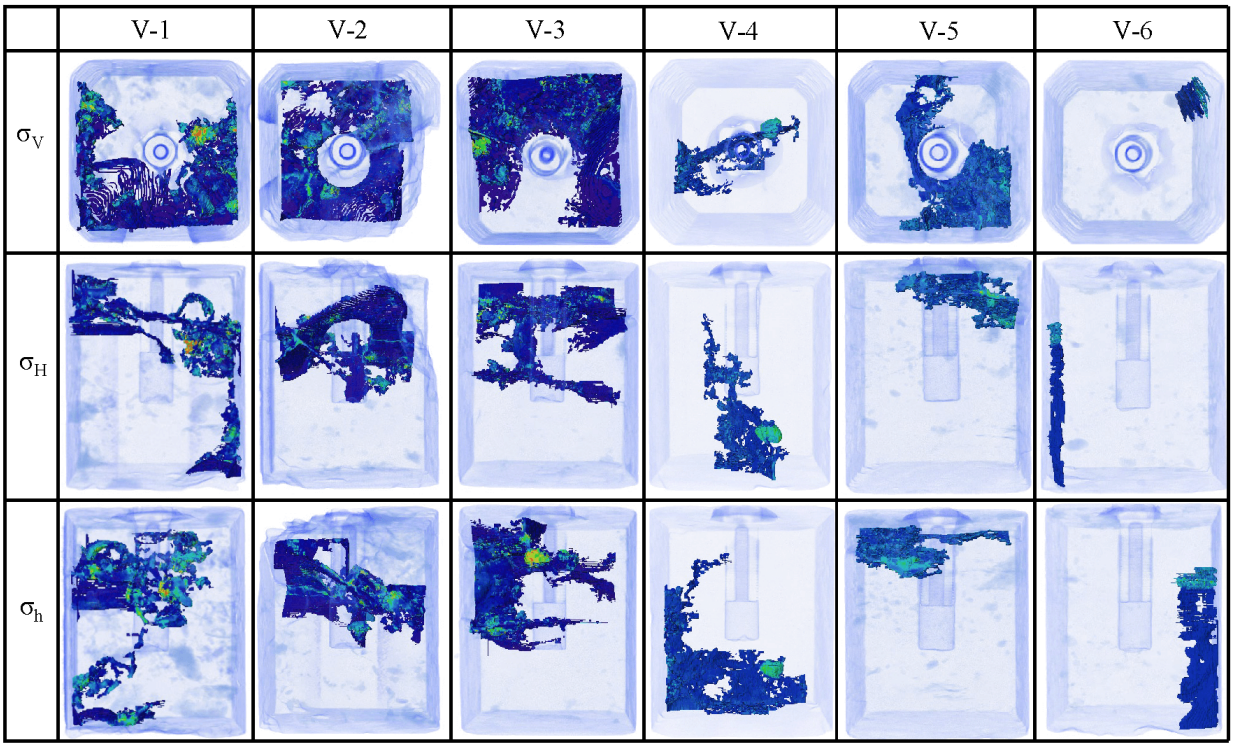

Fig. 2. Reconstructed 3D fractures inside the specimen.

pressure fluctuations were observed during CO_2 fracturing in C2-1, indicating multiple fracture initiations and confirming the presence of numerous branch fractures.

C3-1 exhibited a wide main fracture and several narrower branch fractures. In gravel-rich zones, a fracture belt developed through continuous damage, facilitating effective reservoir stimulation. The formation of a complex fracture network was dominated by a main fracture near the wellbore. The main fracture extended along the maximum horizontal principal stress direction and exhibited good continuity. Branch fractures were predominantly distributed in small gravel-rich zones and propagated through gravels. The formation of branch fractures causes sudden fluid pressure drops (Zhou et al., 2024).

C4-1 exhibited a serrated main fracture with a narrow width. Several closed branch fractures were observed adjacent to the main fracture. The fracture initiated from the wellbore, exhibiting high dispersion, significant tortuosity and poor continuity in the fracture network. The pressure response indicates that CO_2 injection pressure in clay-cemented conglomerate initially increases steadily, then abruptly increases to the breakdown pressure.

C5-1 exhibited predominantly tortuous fractures bypassing gravels. In gravel-rich zones, these fractures had a serrated pattern. A primary fracture propagated along the maximum horizontal principal stress direction. This main fracture was concentrated in the upper portion of the sample and was characterized by good continuity and no obvious secondary branches. Breakdown pressure variations among different conglomerate support types during CO_2 fracturing were negligible, indicating that the support type has minimal impact on the ease of artificial fracture initiation. Matrix-particle-supported conglomerate primarily forms a single main fracture during CO_2 fracturing, whereas particle-supported conglomerate tends to develop multiple branch fractures that bypass gravels.

C6-1 displayed predominantly tortuous fractures traversing gravels. In large gravels, these traversing fractures had serrated profiles and narrow widths. A primary fracture propagated along the maximum horizontal principal stress direction. This main fracture originated distantly from the wellbore and adjacent to the rock surface, indicating that CO_2 infiltrates the rock matrix through pores and microfractures after entering from the wellbore. As CO_2 injection progressed, pressure in the permeation pathways elevated. When the pressure at a specific site on the pathway wall reached the breakdown pressure, fracture initiation and propagation ensued. The higher breakdown pressure in calcite-cemented conglomerates relative to clay-cemented counterparts indicates greater challenges in fracture initiation for the former. Injection pressure in calcite-cemented conglomerate increases steadily until fracture initiation, without sudden pressure surges (Fig. 2).

4. Discussion

4.1 Quantitative analysis of fracture fracturing

The experiment demonstrated that the CO_2 pre-injection + fracturing fluid method yields the largest fracture volume and area, providing the most effective stimulation (Bennour et al., 2015). Calcite-cemented conglomerate exhibits the smallest fracture volume and area after CO_2 fracturing, resulting in the weakest stimulation effect, whereas clay-cemented conglomerate achieves better stimulation with CO_2 fracturing. The

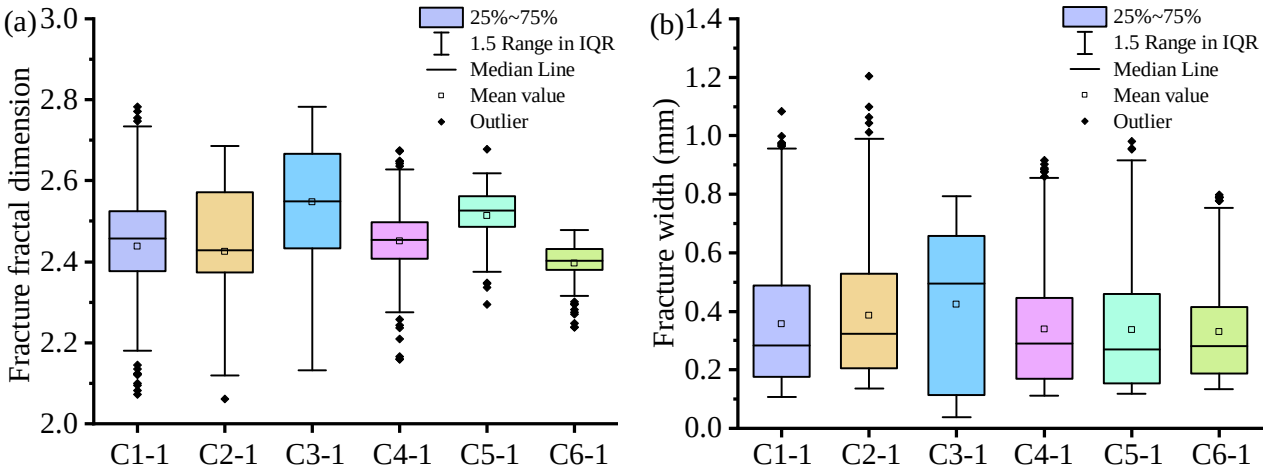

Fig. 3. (a) Fracture fractal dimension and (b) fracture width.

Table 6. Fracture area and volume.

Fracture diameter	C1-2	C2-1	C3-1	C4-1	C5-1	C6-1
Area (cm^2)	126.7328	205.101	306.9571	99.1193	84.8504	26.8376
Volume (cm^3)	6.8488	10.2247	12.0869	5.4307	4.9305	3.1129

Table 7. Comparison of breakdown pressure (MPa).

No.	C1-1	C2-1	C2-1	C3-1	C4-1	C5-1	C6-1
Volue	28.5	27.3	29.8	26.1	23.2	21.1	24.2

conglomerate, composed of gravel, cement and matrix, forms a complex three-phase medium (Table 6). During fracture propagation, fractures may cross, bypass or terminate at gravels, resulting in tortuous and complex fracture geometries. Thus, fluid type and injection sequence do not significantly affect the complexity or width of fracture morphology (Fig. 3). Among different support types, particle-supported conglomerate achieved the best stimulation effect with CO_2 fracturing due to its high gravel content, uniform particle size, and weak inter-gravel cementation. During soaking, CO_2 dissolves cementation interfaces, forming dissolution microfractures, and fractures predominantly propagate by bypassing gravels. In matrix-particle-supported conglomerates, lower gravel content and more variable particle sizes lead to CO_2 dissolving both cementation and matrix among small gravels. Fracture propagation through both gravel and matrix causes rapid CO_2 leak-off, making it difficult to maintain high net pressure in fractures and resulting in weaker stimulation compared to the particle-supported conglomerate.

4.2 Reducing the difficulty of fracturing stimulation

Under identical strain conditions, axial stress evolves more slowly in soaked samples (Fig. 4). This is attributed to the presence of microfractures and dissolution pores in soaked cores. These features undergo compaction during axial loading, leading to a slowed increase in axial stress. Additionally, microfractures and dissolution pores induce stress concentration during triaxial compression testing, accelerating damage accumulation and reducing compressive strength (Ishida et al., 2012). Samples such as C4-2, C5-2, and C6-2, which were exposed to CO_2, exhibited lower peak stress and less stable stress-strain curves compared to their non-exposed counterparts. This reduction in strength is attributed to chemical reactions between CO_2 and the cementing materials – especially in calcium-cemented and multi-stage particle structures-which degrade particle bonding and compromise structural integrity, while this effect was less pronounced in some mudstone-cemented samples. CO_2 exposure overall tended to reduce the strength of gravel rock, particularly under axial stress due to weakened cohesion and the possible dissolution of key mineral components within the microstructure.

Both direct CO_2 fracturing and CO_2 pre-injection followed by slickwater fracturing exhibited higher breakdown pressures than the CO_2-only fracturing group (Table 7). This phenomenon is attributed to the low viscosity and high mobility of CO_2, which enable it to penetrate the microscopic pores in the rock matrix more effectively, leading to enhanced intra-fracture diffusion compared to water-based fluids. In sample C1-1, post-soaking porosity and permeability decreased by 19.5% and 69.1%, respectively. This induced a rapid increase in pore pressure around the fracture during subsequent CO_2 injection, reducing differential stress and promoting fracture initiation with more uniform propagation. Among various conglomerate support types during CO_2 fracturing, the breakdown pressure of particle-supported conglomerate

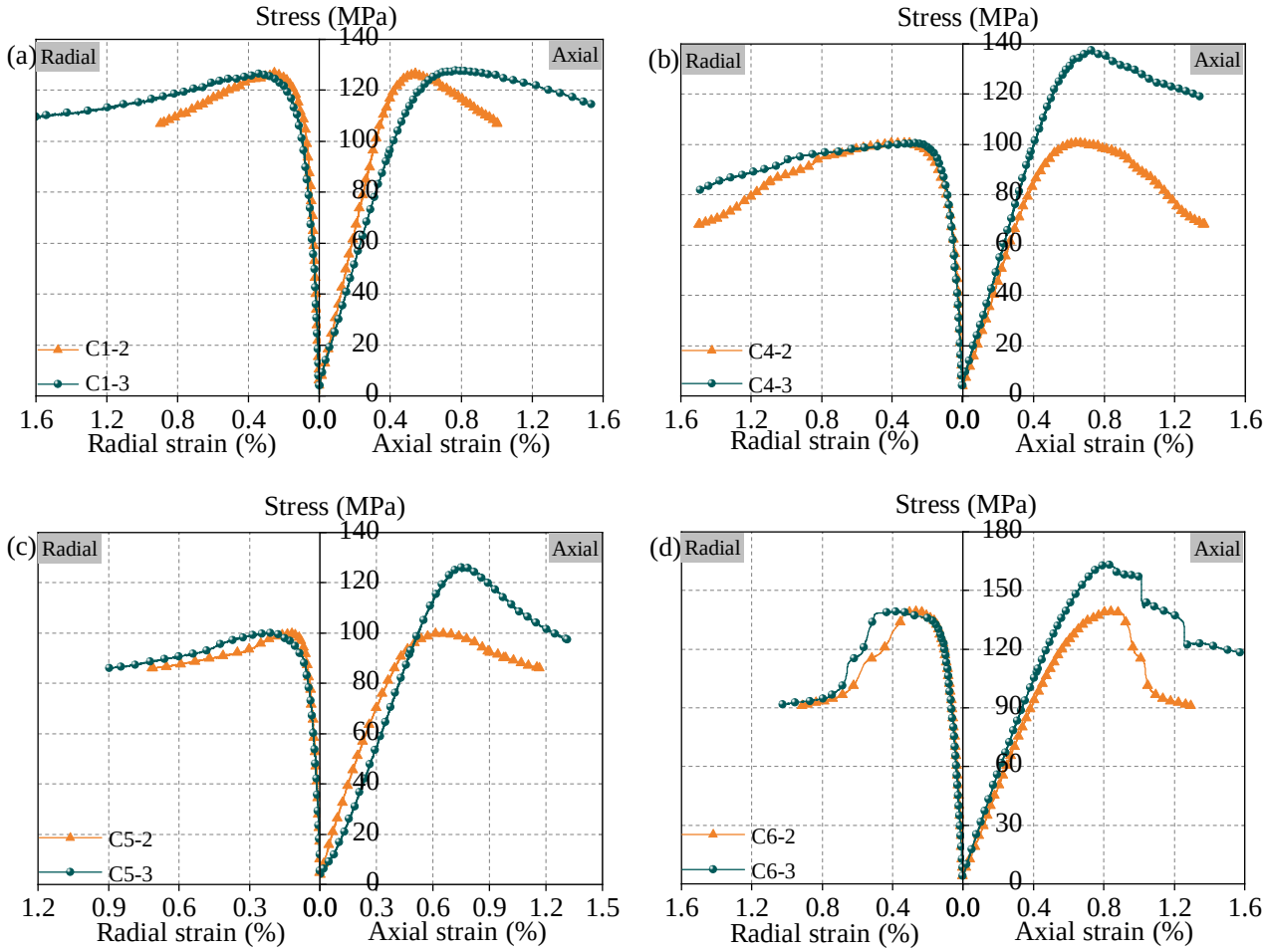

Fig. 4. Triaxial compressive stress-strain curve: (a) C1-2 and C1-3, (b) C4-2 and C4-3, (c) C5-2 and C5-3, and (d) C6-2 and C6-3.

was higher than that of matrix-particle-supported conglomerate. The Young's modulus of particle-supported conglomerate decreased by 23.6%, and its tensile strength decreased by 16.7% after soaking. The Young's modulus and tensile strength for matrix-particle-supported conglomerate decreased by 6.7% and 20%, respectively; the more pronounced plasticity increase in particle-supported conglomerate enhanced its deformation resistance during fracturing. Additionally, particle-supported conglomerate is characterized by high gravel content and uniform particle size. Fractures predominantly propagate around gravels; when reaching the cementation interface between gravels, continuous pressure is required to increase net pressure and form gravel-bypassing fractures, resulting in higher main fracture breakdown pressure. In contrast, CO_2 soaking dissolves numerous cementation interfaces and matrix in matrix-particle-supported conglomerates, forming dissolution microfractures and pores. Fractures tend to penetrate gravels or matrix, requiring less energy for initiation and leading to lower breakdown pressure. CO_2 fracturing induced higher breakdown pressure in calcite-cemented conglomerate than in clay-cemented conglomerate. Post-CO_2 soaking, the compressive strength, tensile strength, and permeability of clay-cemented conglomerate decreased by 18%, 20% and 49.6%, respectively, while those of calcite-cemented conglomerate decreased by 13.3%, 16.1% and 34.4%, respectively. The more significant strength degradation in clay-cemented conglomerate required less stress for failure during CO_2 fracturing. Moreover, the reduction in brittle minerals in calcite-cemented conglomerate (C6-2) was less than that in clay-cemented conglomerate (C4-2) after soaking, leading to lower breakdown pressure in the latter during CO_2 fracturing.

4.3 CO_2 penetration depth

The figures illustrate that the penetration range in each direction is defined by measuring the distance from the wellbore center to the farthest fracture tip in the three-dimensional fracture morphology. The maximum penetration depth in the vertical stress direction is denoted as $L_{v(\max)}$, that in the maximum horizontal principal stress direction as $L_{H(\max)}$, and that in the minimum horizontal principal stress direction as $L_{h(\max)}$. The methodology for extracting fracturing fluid penetration depths in different principal stress directions is illustrated in Fig. 5(a). The extraction results for fracture penetration depths across principal stress directions are shown

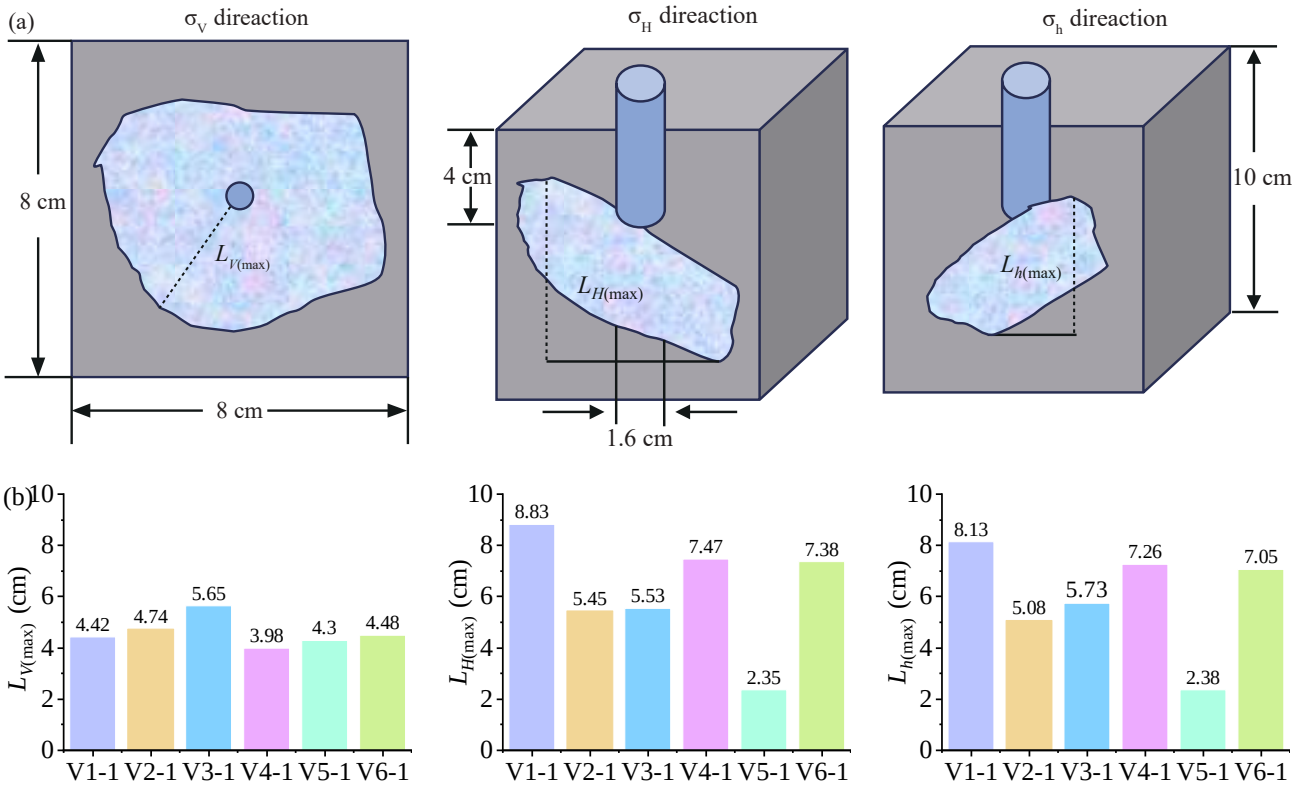

Fig. 5. Results of fracture penetration depths for different principal stress directions: (a) Methodology for extracting fracturing fluid penetration depths in different principal stress directions and (b) extraction results for fracture penetration depths across principal stress directions.

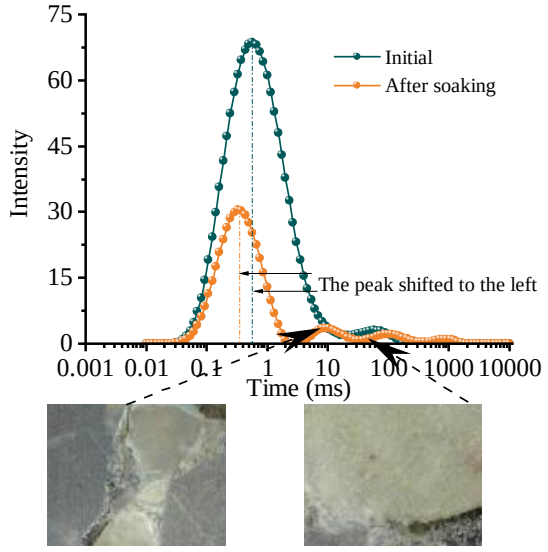

Fig. 6. Test results of T_2 and microscopic analysis.

in Fig. 5(b). In the vertical stress direction, slickwater fracturing exhibits the most significant penetration depth, followed by CO_2 pre-injection fracturing with subsequent slickwater injection. Among the various conglomerate support types, particle-supported conglomerates show the highest penetration depth with CO_2 injection, followed by matrix-particle-supported ones, while multi-size particle-supported conglomerates exhibit the lowest penetration depth.

In conglomerates, CO_2 injection yielded greater penetration depth in calcite-cemented rocks than in clay-cemented rocks. In the maximum horizontal principal stress direction, CO_2 fracturing achieved a greater fracture penetration depth than slickwater fracturing or CO_2 pre-injection followed by slickwater fracturing. Particle-supported conglomerate again demonstrated the highest penetration depth with CO_2, followed by matrix-particle-supported and multi-size particle-supported conglomerates. The penetration depth difference between calcite-cemented and clay-cemented conglomerates under CO_2 injection was minimal (≤ 0.1 cm). In the minimum horizontal principal stress direction, fractures created by CO_2 fracturing exhibited a greater penetration depth than those made by slickwater fracturing or CO_2 pre-injection followed by slickwater. Particle-supported conglomerate showed the highest CO_2-induced penetration depth, followed by matrix-particle-supported and multi-size particle-supported as the lowest. In this direction, the calcite-cemented conglomerate had a lower CO_2 fracturing penetration depth than the clay-cemented conglomerate. Overall, hydraulic fracturing fluid promotes fracture extension in the vertical stress direction, while CO_2 enhances extension in the horizontal principal stress directions. In calcite-cemented conglomerates, CO_2 fracturing results in comparatively restricted fracture penetration depth.

The surface morphology and NMR T_2 spectra of various conglomerate types before and after CO_2 soaking are illus-

trated in Fig. 6. Observations of the core surfaces before and after soaking indicate that intense CO_2 diffusion induces the dissolution of cementation interfaces among gravels (C1-2), the matrix in fine-grained gravel-rich zones (C4-2, C5-2), and the matrix in C6-2. This process gives rise to the formation of dissolution pores and microfractures. Simultaneously, the NMR T_2 spectra of the cores reveal that several small new peaks emerge on the right side of the spectrum after CO_2 soaking, indicating the *in-situ* formation of numerous dissolution pores and microfractures within the core (Mitchell et al., 2013). These dissolution features are principal channels for fracturing fluid leak-off during subsequent hydraulic fracturing. The injected fracturing fluid can rapidly migrate through these preferential flow pathways to deeper rock strata, significantly enhancing the penetration depth of artificial fractures. This further demonstrates that fractures formed by dissolution during soaking dictate the location and penetration depth of subsequent hydraulic fractures.

4.4 Field-scale CO_2 pre-fracturing trial

The results of laboratory experiments revealed that the physicochemical coupling effect of CO_2 injection in conglomerates enhances both the penetration depth and tortuosity of fractures within the reservoir. To further elucidate the role of CO_2 during hydraulic fracturing in the Mahu conglomerate reservoir, a field-scale CO_2 pre-fracturing trial was conducted in a targeted well block. The target formation of the selected implementation wells was the conglomerate reservoir of the Upper Urho Formation, with the main support types being particle-supported and multi-size particle-supported conglomerates. Segmented CO_2 injection was applied in the horizontal test well to evaluate the influence of CO_2 on fracturing performance. Specifically, CO_2 injection was skipped in sections 1, 3, 5, etc., whereas it was performed in sections 2, 4, 6, etc. The test well included 34 fracturing sections, with 200 tons of CO_2 injected into each CO_2-treated section. All other fracturing parameters were kept constant.

The breakdown pressure in CO_2 pre-fracturing sections was significantly lower than in non-CO_2 sections. This finding correlates with the laboratory results, confirming that CO_2 pre-fracturing can effectively reduce breakdown pressure. The net pressure within fractures was also significantly higher in CO_2 pre-fracturing sections compared to non-CO_2 sections. Previous studies have shown that higher net pressure within fractures results in increased fluid pressure acting on reservoir rock, thereby facilitating fracture initiation and propagation. Consequently, higher net pressure leads to more fully developed fractures and a more complex fracture network. The fracture network induced by CO_2 pre-fracturing is more intricate than that by conventional fracturing. In this study, the fracture length, width and fractal dimension in CO_2 pre-fractured samples were greater than those fractured with traditional fluids.

Notably, the pumping pressure in CO_2 pre-fracturing sections was higher, with more pronounced pressure fluctuations. Based on the fracture morphology observed in the laboratory experiments (Figs. 7(a) and 7(b)), CO_2 pre-fracturing produces fractures with higher tortuosity and narrower width. Simultaneously, this technique promotes a deeper penetration of fractures into the reservoir. In summary, during field fracturing, CO_2 pre-injection generates a fracture network characterized by greater penetration depth, narrower width, higher tortuosity, and more branches than conventional fracturing.

Further analysis assessed the impacts of fractures induced by different injection fluids on proppant transport. Building on these findings, Figs. 8(a)-8(c) depict the fracture network induced by slickwater injection, whereas Figs. 8(d)-8(f) illustrate the fracture network generated by CO_2 pre-fracturing. During CO_2 pre-injection, the fluid infiltrates the core and damages the gravel-cementation interfaces, initiating microcracks. In the subsequent fracturing stage, the fractures exhibit enhanced tortuosity and depth but reduced width. Upon infiltration of the proppant-laden fluid into the fractures, rapid fluid leak-off occurs, impeding proppant migration to the fracture tips and causing accumulation near the wellbore, which leads to sandbank formation. Owing to the high tortuosity and friction within the fracture network, the fracturing pressure escalates and exhibits substantial fluctuations during the operation. During sand injection, the elevated friction in tortuous fractures accelerates fluid leak-off, increasing local proppant concentration, forming temporary sand plugs, and elevating intra-fracture fluid pressure. As a result, the injection pressure in the CO_2 pre-fracturing scenario is elevated and displays pronounced fluctuations.

In contrast, in the scenario without CO_2 pre-fracturing, the pre-injection of high-viscosity fluid generates a main fracture with greater width and lower tortuosity. The injected proppant-laden fluid can migrate farther along the main fracture, facilitating more effective proppant placement and fracture support. During sand injection, the fluid pressure remains relatively low and stable.

5. Conclusions

This work aimed at elucidating the physical-chemical coupling mechanisms of CO_2 on rock properties and fracturing behavior across various conglomerate types by conducting CO_2-saturated brine soaking experiments and true triaxial fracturing tests. The physicochemical coupling mechanisms were clarified through quantitative characterization of the mineralogical, pore structure and mechanical property changes, and fracture propagation during CO_2 pre-fracturing. The following conclusions are drawn:

1) CO_2 soaking induces quartz reduction and clay mineral increase, leading to diminished porosity and mechanical strength. Clay-cemented conglomerates experience a greater loss in compressive strength and higher reduction in permeability compared to calcareous-cemented counterparts under identical CO_2 soaking.
2) Particle-supported rocks show the highest penetration depth with CO_2 injection, followed by matrix-particle-supported ones, while multi-size particle-supported rocks exhibit the lowest penetration depth. CO_2 injection achieves greater penetration depth in calcite-cemented rocks than in clay-cemented rocks. In the horizontal

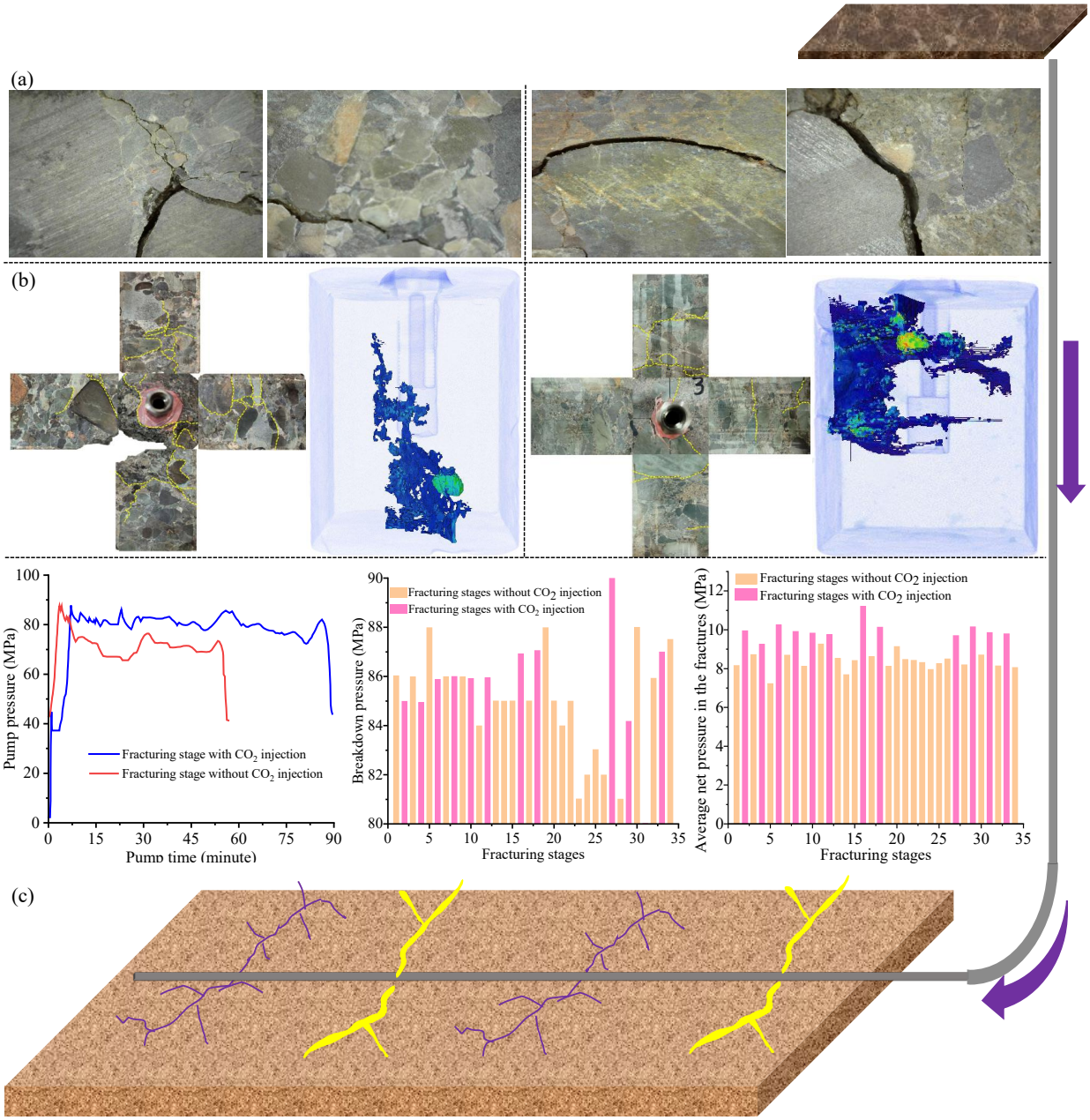

Fig. 7. Analysis of effect of CO_2 fracturing stimulation in the Mahu Conglomerate Reservoir: (a) Microscopic analysis, (b) fracture fracture morphology and (c) real-time pumping pressure curves for CO_2 pre-fracturing and non-CO_2 sections during field operations.

principal stress direction, CO_2 fracturing has a greater fracture penetration depth than slickwater fracturing or CO_2 pre-injection followed by slickwater fracturing. CO_2 pre-fracturing reduces breakdown pressure by 15-5% and increases fracture complexity.

3) Field data confirm that CO_2 pre-injection reduces breakdown pressure by 15% and increases fracture net pressure by $>$ 20% compared to non-CO_2 stages. Laboratory and field results jointly validate the CO_2 pre-fracturing efficacy in reducing operational complexity while enhancing fracture-network complexity and stimulation volume. However, narrower fracture width and higher tortuosity may limit proppant transportation.

Acknowledgements

This work was supported by the National Natural Science Foundation of China (Nos. 52374057 and U23B2084), the "Tianshan Talent" Training Program (No. 2023TSYCCX0004), and the Autonomous Region Key Research and Development Project (No. 2024B01013-1).

Supplementary file

https://doi.org/10.46690/ager.2025.08.02

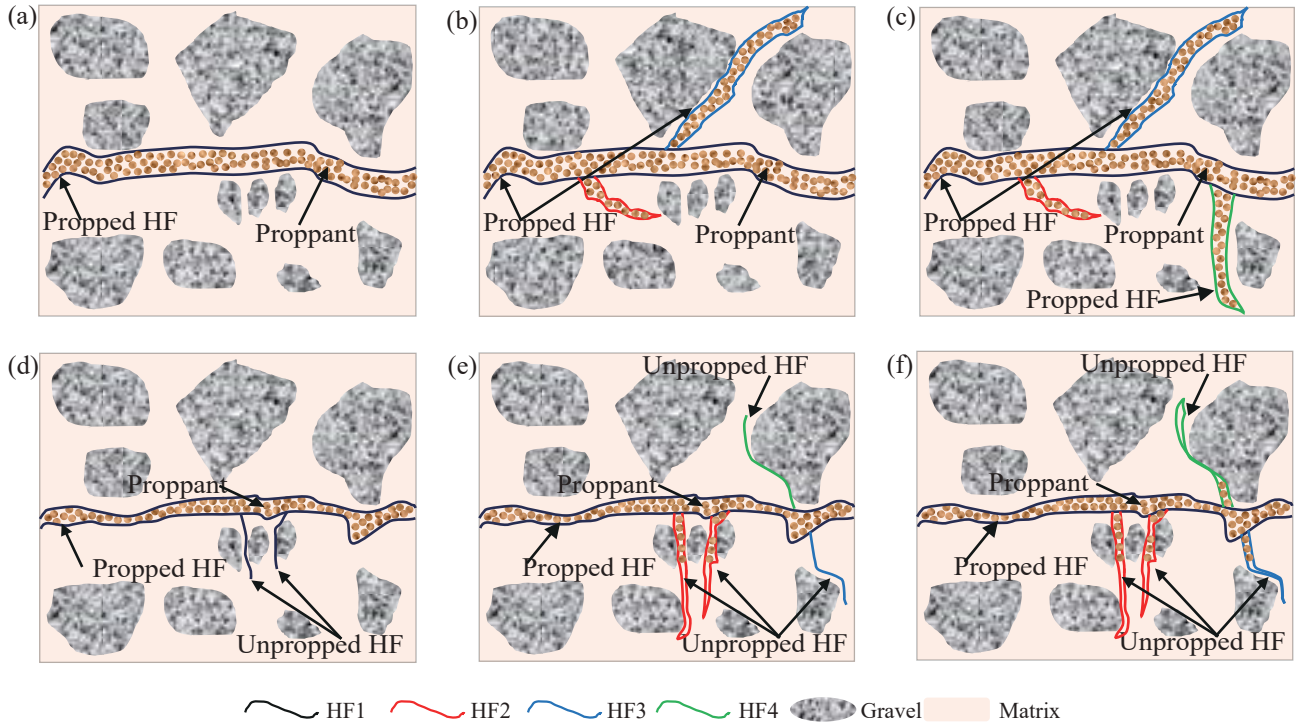

Fig. 8. Schematic diagrams of fracture development and proppant settlement in slickwater and CO_2 fracturing: (a)-(c): Slickwater fracturing and (d)-(f): CO_2 fracturing.

Conflict of interest

The authors declare no competing interest.

Open Access This article is distributed under the terms and conditions of the Creative Commons Attribution (CC BY-NC-ND) license, which permits unrestricted use, distribution, and reproduction in any medium, provided the original work is properly cited.

References

Abes, A., Michael, A. Experimental investigation of geochemical/petrophysical alteration chains from CO_2 injection in dolomitic formations. Journal of Environmental Chemical Engineering, 2025, 13(4): 117102.

Agrawal, S., Sharma, M. M. Practical insights into liquid loading within hydraulic fractures and potential unconventional gas reservoir optimization strategies. Journal of Unconventional Oil and Gas Resources, 2015, 11: 60-74.

Al Kalbani, M., Serati, M., Hofmann, H., et al. Optimizing *in-situ* CO_2 mineralisation: Geomechanics and scalability in dunite and serpentinite rocks-Examples from Australia and New Zealand. Science of The Total Environment, 2024, 927: 172277.

Al-Yaseri, A., Yekeen, N., Al-Mukainah, H. S., et al. Rock-wettability impact on CO_2-carbonate rock interaction and the attendant effects on CO_2 Storage in carbonate reservoirs. Journal of Natural Gas Science and Engineering, 2022, 104: 104664.

Barnaji, M. J., Pourafshary, P., Rasaie, M. R. Visual investigation of the effects of clay minerals on enhancement of oil recovery by low salinity water flooding. Fuel, 2016, 184: 826-835.

Bennour, Z., Ishida, T., Nagaya, Y., et al. Crack extension in hydraulic fracturing of shale cores using viscous oil, water, and liquid carbon dioxide. Rock Mechanics and Rock Engineering, 2015, 48(4): 1463-1473.

Boggs, S. Jr. Principles of Sedimentology and Stratigraphy. London, UK, Pearson Education, 2014.

Chen, H., Kang, Y., Jin, W., et al. Numerical modeling of fracture propagation of supercritical CO_2 compound fracturing. Journal of Rock Mechanics and Geotechnical Engineering, 2024, 16(7): 2607-2628.

de Jong, S. M., Spiers, C. J., Busch, A. Development of swelling strain in smectite clays through exposure to carbon dioxide. International Journal of Greenhouse Gas Control, 2014, 24: 149-161.

De Silva, G. P. D., Ranjith, P. G., Perera, M. S. A., et al. An experimental evaluation of unique CO_2 flow behaviour in loosely held fine particles rich sandstone under deep reservoir conditions and influencing factors. Energy, 2017, 119: 121-137.

Fairhurst, C. On the validity of the 'Brazilian' test for brittle materials. International Journal of Rock Mechanics and Mining Sciences & Geomechanics Abstracts, 1964, 1(4): 535-546.

Feng, Y., Firoozabadi, A. Phase-field simulation of hydraulic fracturing by CO_2 and water with consideration of thermoporoelasticity. Rock Mechanics and Rock Engineering, 2023, 56(10): 7333-7355.

Galdeano, C., Cook, M. A., Webber, M. E. Multilayer geospatial analysis of water availability for shale resources

development in Mexico. Environmental Research Letters, 2017, 12(8): 084014.

Ha, S. J., Choo, J., Yun, T. S. Liquid CO_2 fracturing: Effect of fluid permeation on the breakdown pressure and cracking behavior. Rock Mechanics and Rock Engineering, 2018, 51(11): 3407-3420.

Haimson, B. Micromechanisms of borehole instability leading to breakouts in rocks. International Journal of Rock Mechanics and Mining Sciences, 2007, 44(2): 157-173.

Huang, L., He, R., Yang, Z., et al. Exploring hydraulic fracture behavior in glutenite formation with strong heterogeneity and variable lithology based on DEM simulation. Engineering Fracture Mechanics, 2023, 278: 109020.

Ishida, T., Aoyagi, K., Niwa, T., et al. Acoustic emission monitoring of hydraulic fracturing laboratory experiment with supercritical and liquid CO_2. Geophysical Research Letters, 2012, 39(16): 7705-8370.

Ishida, T., Chen, Y. Q., Bennour, Z., et al. Features of CO_2 fracturing deduced from acoustic emission and microscopy in laboratory experiments. Journal of Geophysical Research: Solid Earth, 2016, 121(11): 8080-8098.

Kanakiya, S., Adam, L., Esteban, L., et al. Dissolution and secondary mineral precipitation in basalts due to reactions with carbonic acid. Journal of Geophysical Research: Solid Earth, 2017, 122(6): 4312-4327.

Kar, S., Chaudhuri, A. Influence of flow and geomechanics boundary conditions on hydraulic fracturing pattern and evolution of permeability between the wells. Engineering Fracture Mechanics, 2024, 298: 109949.

Khanlari, G. R., Heidari, M., Noori, M., et al. The effect of petrographic characteristics on engineering properties of conglomerates from Famenin Region, Northeast of Hamedan, Iran. Rock Mechanics and Rock Engineering, 2016, 49(7): 2609-2621.

Li, W., Frash, L. P., Carey, J. W., et al. Injection parameters that promote branching of hydraulic cracks. Geophysical Research Letters, 2021, 48(12): e2021GL093321.

Li, Y., Zhu, Y., Li, Z., et al. Shale oil recovery by CO_2 injection in Jiyang Depression, Bohai Bay Basin, East China. Petroleum Exploration and Development, 2024, 51(4): 981-992.

Liu, K., Sheng, J., Zhang, Z. A simulation study of the effect of clay swelling on fracture generation and porosity change in shales under stress anisotropy. Engineering Geology, 2020, 278: 105829.

Min, Y., Jun, Y. Anorthite dissolution under conditions relevant to subsurface CO_2 injection: effects of Na^+, Ca^{2+}, and Al^{3+}. Environmental Science & Technology, 2016, 50(20): 11377-11385.

Mitchell, J., Chandrasekera, T. C., Holland, D. J., et al. Magnetic resonance imaging in laboratory petrophysical core analysis. Physics Reports, 2013, 526(3): 165-225.

Mukhametdinova, A., Karamov, T., Markovic, S., et al. Exploring *in-situ* combustion effects on reservoir properties of heavy oil carbonate reservoir. Petroleum Science, 2024, 21(5): 3363-3378.

Nooraiepour, M., Polański, K., Masoudi, M., et al. Potential for 50% Mechanical Strength Decline in Sandstone Reservoirs Due to Salt Precipitation and CO_2-Brine Interactions During Carbon Sequestration. Rock Mechanics and Rock Engineering, 2025, 58(1): 1239-1269.

Patton, B. J., Pitts, F., Goeres, T., et al. Matrix acidizing case studies for the point arguello field. Paper SPE 83490 Presented at the SPE Western Regional/AAPG Pacific Section Joint Meeting, Long Beach, California, 19-24 May, 2003.

Perera, M. S. A., Ranjith, P. G., Peter, M. Effects of saturation medium and pressure on strength parameters of Latrobe Valley brown coal: Carbon dioxide, water and nitrogen saturations. Energy, 2011, 36(12): 6941-6947.

Rathnaweera, T. D., Ranjith, P. G., Perera, M. S. A., et al. An experimental investigation of coupled chemico-mineralogical and mechanical changes in varyingly-cemented sandstones upon CO_2 injection in deep saline aquifer environments. Energy, 2017, 133: 404-414.

Trivedi, J., Babadagli, T. Efficiency analysis of greenhouse gas sequestration during miscible CO_2 injection in fractured oil reservoirs. Environmental Science & Technology, 2008, 42(15): 5473-5479.

Wang, J., Ge, H., Liu, J., et al. Effects of gravel size and content on the mechanical properties of conglomerate. Rock Mechanics and Rock Engineering, 2022, 55(4): 2493-25020.

Warren, P. H., Taylor, G. J., Keil, K., et al. Petrology and chemistry of two "large" granite clasts from the Moon. Earth and Planetary Science Letters, 1983, 64(2): 175-185.

Wu, Y., Tao, J., Wang, J., et al. Experimental investigation of shale breakdown pressure under liquid nitrogen pre-conditioning before nitrogen fracturing. International Journal of Mining Science and Technology, 2021, 31(4): 611-620.

Zhou, H., Wang, B., Zhang, L., et al. Quantitative characterization and fracture morphology in reservoirs with various lithologies: An experimental investigation. Geoenergy Science and Engineering, 2024, 239: 212911.

Zhou, H., Yan, T., Ma, C. et al. Characteristics of propped fracture propagation in volcanic clastic reservoirs: a multiscale study of conductivity sustainability and fracture vetwork complexity. Rock Mechanics and Rock Engineering, 2025, 58(3): 1721-1735.